Barium Titanate BaTiO3 Raman Spectra and their deconvolution with q-BWF functions

Barium Titanate $BaTiO_3$ Raman Spectra and their deconvolution with q-BWF functions

Amelia Carolina Sparavigna

Department of Applied Science and Technology, Polytechnic University of Turin, Italy

amelia.sparavigna@polito.it

Here we study the Raman spectra of Barium Titanate, $BaTiO_3$, given in the RRUFF and ROD databases. Being the Raman bands strongly asymmetric, we are deconvoluting them by means of the q-BWF functions. These functions are generalizing the Breit-Wigner-Fano line shape in the framework of the q-exponential function of Tsallis statistics. Besides the deconvolution of Raman spectra, we consider the literature on $BaTiO_3$ Raman spectroscopy, particularly the assignment of the bands. Being the wavenumbers of some A_1 and E modes very close, the observed modes are mixed. Moreover, dips in the spectra have suggested as due to the presence of anharmonicity, interference and Fano resonance.

Introduction

As explained by Parmar et al., 2023, the perovskites, materials with chemical formula ABX_3 (A and B cations, X anion), have the specific features proper for their use in solar cells. Moreover, "the oxide perovskite semiconductors have outstanding ferroelectric characteristics" (Parmar et al., 2023). "The first material to ever demonstrate ferroelectric capabilities is $BaTiO_3$ [barium titanate], which is in the tetragonal phase at a temperature of about 120 °C and has a special structure known as the ABO_3 perovskites crystal" (Parmar et al., 2023). According to Parmar and coworkers. besides ferroelectricity $BaTiO_3$ is characterized by piezoelectricity, and it possesses a high dielectric constant, and "a high band gap and low current loss". Because of these features, the material has applications "in sensors, actuators, waveguides, high-capacity computers, laser frequency doubling, nanoelectronic devices, … $BaTiO_3$ is well suited for … ferroelectric memristors, multilayer ceramic capacitive transducers, infrared detectors, energy storage devices and various functional actuators" (Parmar et al., 2023).

"Barium titanate was one of the first useful piezoelectric materials, developed in the 1940s and 1950s. Although this material does not have a very high piezoelectric constant, it has a very high permittivity, making it a good material for capacitors. ... [Barium titanate] exhibits a relatively low Curie temperature, however, and therefore has not seen many developments in recent years for applications in piezoelectric devices" (Aksel and Jones, 2010). The barium titanate can be synthesized as a white powder of nanoparticles or as a transparent large crystal. The solid exists in one of four polymorphisms depending on temperature. From high to low temperature, the crystal symmetries are cubic, tetragonal, orthorhombic and rhombohedral crystal structure. In the Fig.2 by Aksel and Jones, we can see the diagrams of the polymorphic phase transitions in barium titanate single crystals, of the spontaneous polarization and dielectric constant changing with temperature. "The low Curie temperature of barium titanate results from the tetragonal to paraelectric cubic phase transition at 120 °C. Barium titanate undergoes several additional structural phase transitions upon decreasing temperature, ... recent studies by Wada et al. on single crystal barium titanate found that these phase transitions can also be induced by applied electric field" (Aksel and Jones, 2010).

"$BaTiO_3$ is known to undergo a ferroelectric transition at ~120 °C ... Above transition temperature, $BaTiO_3$ has cubic (O^1_h or *Pm3m*) symmetry with all oxygen atoms at 3c sites (Wyckoff notation), which have 4/mmm symmetry. Below transition temperature, $BaTiO_3$ has tetragonal (C^1_{4V} or *P4mm*) symmetry with two non-equivalent oxygen sites denoted as O_I and O_{II}" (Zhang et al., 2011).

As previously told barium titanate is in the form of nanoparticles or crystals. To investigate the crystals and the powders of nanoparticles, Raman spectroscopy is fundamental. Here we consider some literature about the Raman spectroscopy on $BaTiO_3$.

Polarized Raman spectroscopy

"Polarized Raman spectra of tetragonal $BaTi0_3$ have been obtained at room temperature … [excitation laser 633 nm] … Using several different crystallographic directions for the phonon wave vector q, most of the vibrational modes for q ~ 0 have been classified using Raman data alone. Three pairs of longitudinal transverse A_1 modes have been observed with frequencies which semiquantitatively satisfy the Lyddane Sachs-Teller relationship. A low-frequency transverse E mode has been observed at 10 cm^{-1} and assigned to the ferroelectric soft-mode system. The soft-mode result has been discussed in terms of the effect of damping on the dispersion relation" (Rimai et al., 1968).

In Jiang et al., 1996, too, we can find *polarized Raman spectra* given over the wavenumber range 100-1600 cm^{-1}. The researchers measured the Raman spectra on single domain crystals. "Numerous independent investigations have demonstrated that two broad asymmetric bands peaked approximately at 275 and 514 cm^{-1} in the A_1(TO) Raman spectrum"; Jiang and coworkers have found "three new weak bands at 986, 1204 and 1480 cm^{-1} in the Raman spectra of $BaTiO_3$ ... According to the temperature dependence of the Raman scattering intensity and bandwidth, [these bands] are attributed to the second-order Raman spectra of $BaTiO_3$ and the strong bands at 275 and 514 cm^{-1} in the A_1(TO) spectrum are confirmed to be of first order. These facts support the order-disorder model of the ferroelectric phase transitions" (Jiang et al., 1996).

Nanoparticles

Let us pass from crystals to nanoparticles. "Barium titanate nanoparticles were synthesized via a low temperature sol-gel technique using acetylacetone as a chelating agent. The X-ray diffraction pattern confirmed the formation of tetragonal perovskite structure of the material. The average crystallite size was found to be 49 nm … Raman spectroscopic features typical for the tetragonal phase were identified for barium titanate powder. … Barium titanate displays polychromatic luminescent peaks in UV-visible regions, and it was attributed to the near-band-edge transition and defect states in the optical band gap of the perovskite structure" (Sherlin Vinita et al., 2022).

"The Raman spectrum of $BaTiO_3$ nanoparticles prepared by sol-gel method is presented in Figure 5 [of Sherlin Vinita et al. article]. The Raman bands (position and intensity) noticed in the range of 160–720 cm^{-1} can be assigned to $BaTiO_3$ nanoparticles" (Sherlin Vinita and coworkers mentioning Scalabrin et al., 1977). "All the Raman optically active modes in the tetragonal phase can be represented by $3[A_1(TO) + A_1(LO)] + B_1 + 4[E(TO) + E(LO)]$ modes" (Sherlin Vinita and coworkers are referring to a Ref.38, an article with wrong authors' names; DOI corresponds to Bahri & Khemakhem, 2014). For nanoparticles, the researchers find four dominant bands with positions at 237, 296, 506, and 714 cm^{-1}. "More than one phonon modes are available for each Raman bands, since the wavenumbers of some A_1 and E modes are very closer, consequently the observed modes are mixed" (Sherlin Vinita and coworkers mentioning Pasha et al., 2007). "Additionally, Raman spectrum of the tetragonal $BaTiO_3$ phase contains *negative dips* at 158 cm^{-1} and 442 cm^{-1} (E (TO), E(LO)). Scalabrin et al. interpreted this latter effect as overdamped mode due to the interference of the TO modes, while Venkateswaran et al. interpreted it as an interference due to the anharmonic coupling between the A_1(TO) phonons. The tetragonal phase can be confirmed by noticing the relative intensity of the bands at 296 and 714 cm^{-1}. The Raman band appeared at 296 cm^{-1} is assigned to the B_1 mode, suggesting asymmetry within the $[TiO_6]$ octahedral, while the Raman band located at 714 cm^{-1} is related to the LO mode of A_1 symmetry. In fact, these bands are absent in the cubic phase" (Sherlin Vinita and coworkers mentioning Sendova et al., 2016, Maxim et al., 2011).

A band at 1080 cm^{-1} is assigned to $BaCO_3$ impurity. The position of the Raman bands in the work by Sherlin Vinita and coworkers "is different when compared to previous reports due to the synthesis method" (see references in Sherlin Vinita et al.). In previous literature Raman bands have been observed at 250, 307, 520 and 720 cm^{-1} for material prepare by solvothermal method (Lee, et al., 2012). In Shiratori et al., Raman active bands are at 257, 306, 517 and 715 cm^{-1}. Other works give Raman bands at 260, 305, 515 and 715 cm^{-1} (Hayashi et al.), at 260, 305, 520 and 715 cm^{-1} (Huang et al.), and at 254, 307, 518 and 713 cm^{-1} (Sun et al., see discussion Sherlin Vinita et al. and references therein).

237, 296, 506, and 714 cm^{-1} Sherlin Vinita et al.

257, 306, 517, and 715 cm^{-1} Shiratori et al.

Sherlin Vinita and coworkers note a red shift in Raman bands they observed as due ""to the localized tensile strain in the material".

Powders

In the abstract by Shiratori et al., 2007, we can read "$BaTiO_3$ powders with various crystallite sizes, which were prepared through microemulsion-mediated synthesis, were thoroughly studied by Raman spectroscopy. Clear evidence for the presence of the tetragonal phase was found for ultrafine powders with an average crystallite size above 30 nm. … In particles as fine as 100 nm, the short mean free path of phonons, mainly due to internal pressure, causes decoupling of the coupled A_1(TO) phonons and a diffuse phase transition behaviour (T_C = 115°C). Coupled A_1(TO) phonons, which give a spectral dip at around 180 cm^{-1} and a lesser extent of diffuseness, were revealed for powders consisting of particles as large as 0.17 μm (T_C = 123°C). Further coarsening upon annealing induced the formation of aggregates, resulting in the shift of phase transition points to higher temperatures for the rhombohedral to orthorhombic and the orthorhombic to tetragonal transitions and to lower temperatures for the tetragonal to cubic transition, respectively" (Shiratori et al., 2007). The researchers investigated the Raman spectra by means of a Jobin-Yvon T64000 Raman spectrometer and a Spectrum One CCD detection system. The powder samples were excited with laser radiation at 514.5 nm.

"Figure 4 [in Shiratori et al.] shows the evolution of Raman spectra obtained for powders annealed at various temperatures". The plots are "typical depolarized scattering profiles for single and polycrystalline $BaTiO_3$" (Shiratori et al., mentioning Noma et al., 1996, Venkateswaran et al., 1998). The Raman active phonons of tetragonal P4mm crystal symmetry are represented by $3A_1+B_1+4E$. "Long-range electrostatic forces induce the splitting of transverse and longitudinal phonons, … The detailed phonon assignments are indicated on the spectrum", in the Fig. 4(j) by Shiratori et al. "It is well known that the $BaTiO_3$ tetragonal phase reveals Raman scattering bands at around 250, 520 and 720 cm^{-1} and a sharp peak at around 306 cm^{-1}. On the other hand, … Although the cubic phase theoretically does not reveal any Raman active modes, this polymorph generally shows broad bands at around 250 and 520 cm^{-1}, which may be caused by local disorder associated with the position of Ti atoms". "The raw powder emits a very intense background, which is probably fluorescence originating from the organic residues … a mixture of Raman scattering features for cubic and tetragonal $BaTiO_3$ can be observed at around 297, 523 and 720 cm^{-1}". Note that the inset of Fig. 4(a) is showing a Raman spectrum processed by a baseline correlation. The proposed spectrum "indicates that the as-synthesized powder is already crystallized in a mixture of a dominant cubic and a very minor tetragonal portion since the intensity of the tetragonal features is very low" (Shiratori et al., 2007).

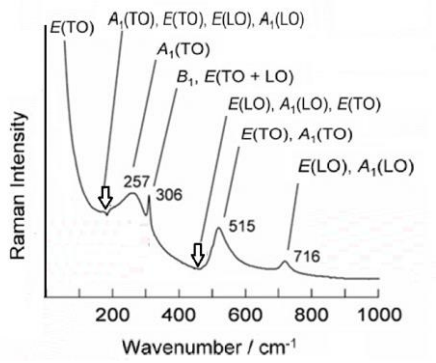

Fig.1: A Raman spectrum adapted from Shiratori et al., 2007. Note the two dips, indicated by the arrows.

According to Shiratori and coworkers, "Raman spectroscopy reveals a clear evidence for local tetragonality for particles as small as 20–30 nm. … Powders annealed at temperatures above 900°C show a clear spectral dip at around 180 cm^{-1}. This dip is known to appear for depolarized single crystals and polycrystalline samples at room temperature owing to the *anharmonic coupling* among three A_1(TO) phonons" (Shiratori et al., 2007). In particular, "with increasing annealing temperature (and simultaneously crystallite size), a peak at around 180–186 cm^{-1} gradually transformed into a dip at 179 cm^{-1} because of the anharmonic coupling among the A_1(TO) phonons". For the anharmonic coupling, Shiratori and coworkers are referring to Venkateswaran et al., 1998.

Pressure

Let us consider Venkateswaran et al., 1998, where Raman peaks are assigned, as in Shiratori et al, "to more than one phonon mode". The Table I in Venkateswaran et al. is giving the optical phonon frequencies and their mode symmetry assignments in tetragonal $BaTiO_3$ as from literature (see please the references therein). Here the frequencies (cm^{-1}):

36 170 180 185 270 305 305 463 475 486 518 520 715 720

Figure 1 in Venkateswaran et al. is showing the room temperature spectra of $BaTiO_3$ polycrystalline powder for different pressures, "between atmospheric pressure and 3.5 GPa. The dominant features in the 1 bar … are a broad peak centered near 265 cm^{-1} [A_1(TO)], a sharp peak at 315 cm^{-1} [B1, E(TO,LO)], an asymmetric and broad peak near 520 cm^{-1} [A_1, E(TO)], and a broad, weak peak at around 720 cm^{-1} [A_1, E(LO)], … . The observed Raman peaks have been assigned to more than one phonon mode since the frequencies of a few A_1 and E modes are very close (see Table I [in Venkateswaran et al., 1998]) and *also the different orientations of the crystallites in a polycrystalline sample does not permit polarization* selection between the A_1 and E modes. The observed spectrum at 1 bar agrees well with the powder Raman spectrum reported by Burns and Scott and also with those reported for ceramic and polycrystalline films grown by metal-organic chemical vapor deposition" (Venkateswaran et al., and references therein). "It compares well with the single crystal data except for a dip near 186 cm^{-1} which has been understood as an interference due to the anharmonic coupling between the three A_1(TO) phonons"; in a note Venkateswaran and coworkers write that "the dip at 186 cm^{-1} has been observed in [their] samples when the Rayleigh tail at low frequencies was reduced considerably".

It is time to plot spectra and propose a deconvolution of them.

RRUFF and ROD databases

We can find $BaTiO_3$ spectra in RRUFF and ROD databases (Lafuente et al., 2015, El Mendili et al., 2019). We will deconvolve the available spectra using q-BWF functions (Sparavigna, 2023). The term "deconvolution" is largely used in Raman spectroscopy; its meaning is that of a decomposition in components of the spectrum. We proposed the q-BWF function as a generalization of the Breit-Wigner-Fano (BWF) line

shape, to obtain an asymmetric form of the q-Gaussian function. The BWF line shape is a modified Lorentzian (Breit-Wigner) function, which is used to consider the asymmetry due to Fano resonance. The generalization we proposed in 2023 is using, in the BWF line, a q-Gaussian line shape instead of a Lorentzian profile. A q-Gaussian is a function based on the Tsallis q-form of the exponential function (Tsallis, 1988); this generalized exponential is characterized by a q-parameter and when q is equal to 2, we have the Lorentzian function. If q is close to 1, we have a Gaussian function. For values of q between 1 and 2, we have a bell-shaped function with power-law wings ranging from Gaussian to Lorentzian tails. As shown on many occasions, the q-Gaussian is suitable for fitting Raman spectra, such as the q-BWF functions (see Sparavigna, 2024, and references therein).

Let us write the BWF as follow: $BWF = C\left[1 - \xi\gamma^{1/2}(x - x_o)\right]^2 [1 + \gamma(x - x_o)]^{-1}$, where x_o is the center of the line. When parameter ξ is zero, *BWF* becomes a Lorentzian function. Therefore, it is easy to turn BWF into a q-BWF function: $q\text{-}BWF = C\left[1 - \xi\gamma^{1/2}(q-1)^{1/2}(x - x_o)\right]^2 [1 + (q-1)\gamma(x - x_o)^2]^{1/(1-q)}$.

Please consider that in literature about Fano resonance the parameter ξ is often given as 1/q (and with an opposite sign). Here the q-parameter is related to the Tsallis statistics. The *q-BWF* functions have been applied to the study of the Raman spectra of molybdenite, that is, the molybdenum disulfide, MoS_2, using the Raman spectra from RRUFF database. Then, we applied q-BWFs to RRUFF spectra of rare-earth oxide REO glasses.

For the decomposition of spectra, we use software Fityk. In it, a q-Gaussian function can be defined in the following manner: define Qgau(height, center, hwhm, q=1.5) = height*(1+(q-1)*((x-center)/hwhm)^2)^(1/(1-q)) , where q=1.5 is the initial guessed value of the q-parameter. Parameter hwhm is the half width at half maximum of the component. And the q-BWF as:

define Qbreit(height, center, hwhm, q=1.5, xi=0.1) = (1-xi*(q-1)*(x-center)/hwhm)^2 * height*(1+(q-1)^0.5 *((x-center)/hwhm)^2)^(1/(1-q)) .

RRUFF R110180 - Two spectra are available for Barium Titanate; the given name of mineral is Barioperovskite (see Ma & Rossman, 2008). Ideal Chemistry: BaTiO3. Locality: Synthetic. Source: Guangtian Zou, Owner: RRUFF. Status: The identification of this mineral has been confirmed by single-crystal X-ray diffraction. Mineral Group: Perovskite.

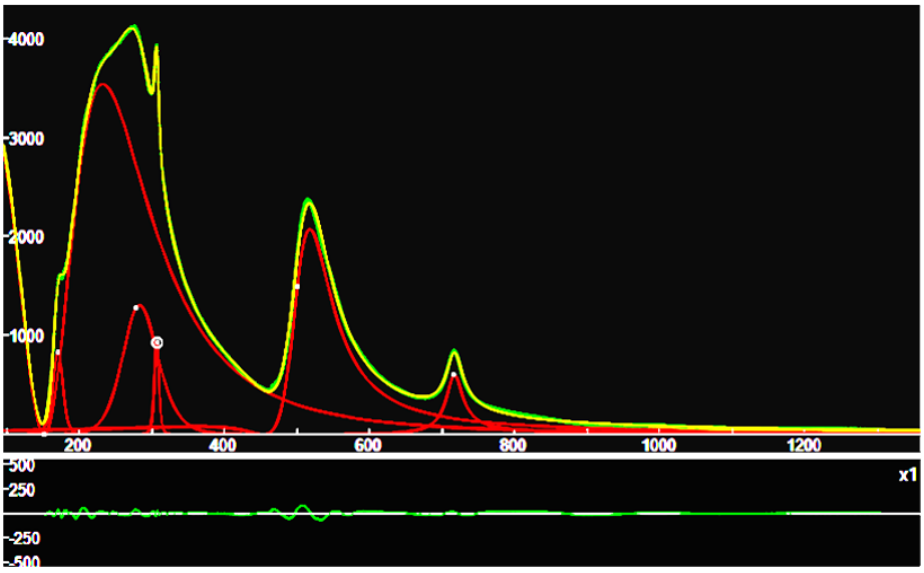

Fig.2: *Raman spectrum RRUFF R110180 (green), laser 532 nm, decomposed in q-BWF functions (red curves). The x-axis is representing the Raman shift (cm^{-1}). The sum of these components is given in yellow. In fact, green data and yellow line are practically undistinguishable. In the lower part of the image, the misfit is given, that is, the difference between green data and yellow line.*

As for the BWF, also for q-BWF functions the center of the line does not coincide with the peak of the component. In the Figure 2, the peaks of the components are at 171, 230, 285, 308, 518, and 718 cm−1.

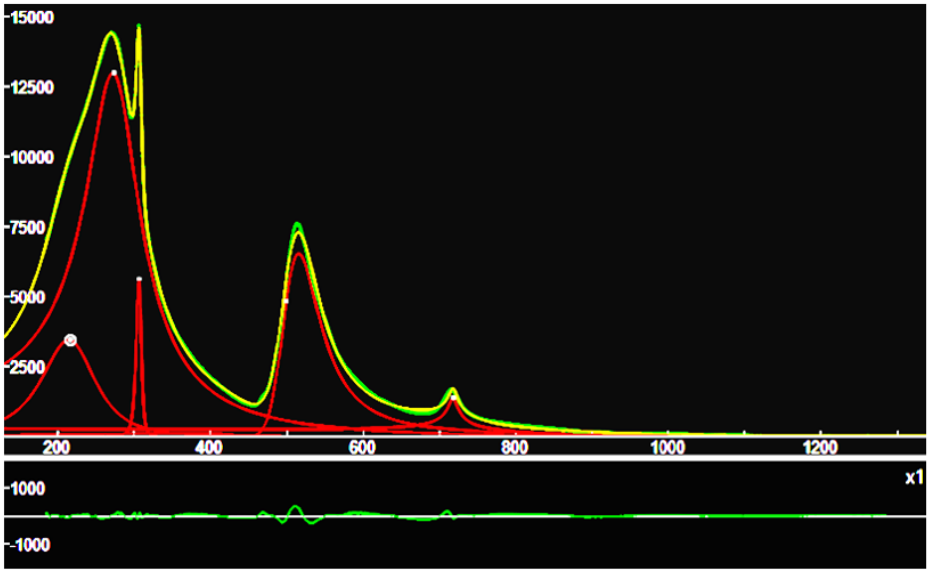

Fig.3: *Raman spectrum RRUFF R110180 (green), laser 780 nm, decomposed in q-BWF functions (red curves). The x-axis is representing the Raman shift (cm^{-1}). Yellow line is the sum of components. The lower part of the image is representing the misfit.*

In the Figure 3, the peaks of the components are at 215, 272, 305, 515, and 718 cm^{-1}.

ROD 3500224 - Let us pass to spectrum 3500224 in ROD database. Sample commercial CRICERAM pur. Information: Excitation wavelength 633 nm, Measurement resolution 1 cm^{-1}, Polarization direction: unoriented, Power on sample 0.6 mW, Spot size of the device 1.5 μm, Company of the measurement device Horiba LabRamHR800.

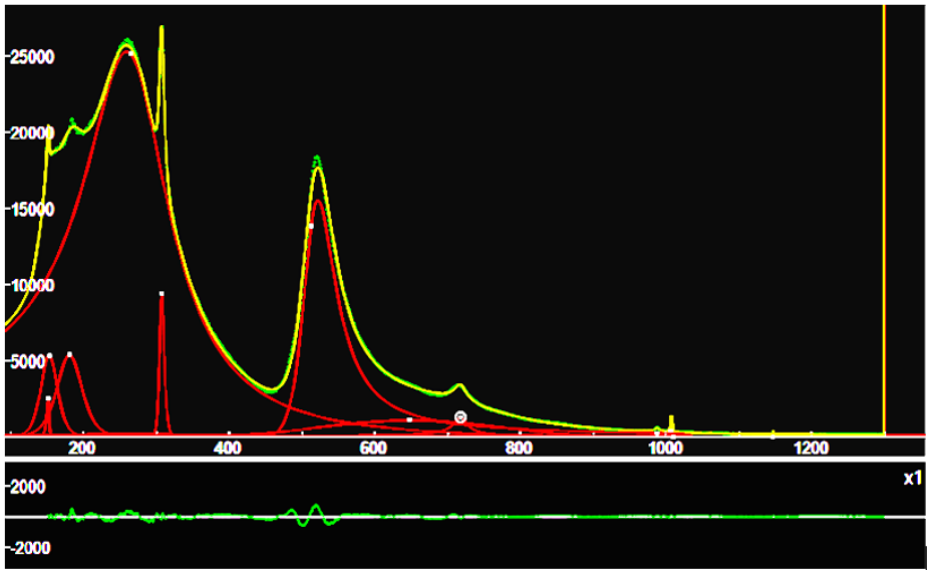

Fig.4: *Raman spectrum ROD 3500224 (green), laser 633 nm, decomposed in q-BWF functions (red curves). Yellow line is the sum of components. The lower part of the image is representing the misfit.*

The peaks are at 147, 152, 177, 258, 307, 522 and 720 cm^{-1}. Considering the three spectra here decomposed and the previously seen literature, we have (cm^{-1}):

		171			230	285	308			518			718	(RRUFF, 532 nm)
				215	272		305			515			718	(RRUFF,780 nm)
147	152	177			258		307				522		720	(ROD, 633 nm)
		170	180	185	270		305	463	475	486	518	520	715 720	(Venkateswaran et al., 1998)
				237	296					506			714	(Sherlin Vinita et al.)
					257		306				517		715	(Shiratori et al.)

Discussion

We used the q-BWF functions to have the possibility of decomposing the spectrum in a few components. As we can clearly see, the bands are strongly asymmetric.

Literature tells us that wavenumbers of some A_1 and E modes are very close, and therefore the observed modes are mixed. For instance, the peak at 515 in the Fig.1, is given as E(TO), A_1(TO). In the Figure 2, we used one q-BWF function for this component. Let us try to decompose it in two different components; we find the following result (on the right, Fig.5), compared to the case with one component (on the left, Fig.5). Note that the misfit (lower part of images) is strongly reduced. The two components have the peaks at 514 and 526 cm^{-1}, respectively. The fit of the dip, that in the Figure 1 is assigned to E(LO), A_1(LO), E(TO) is improved too.

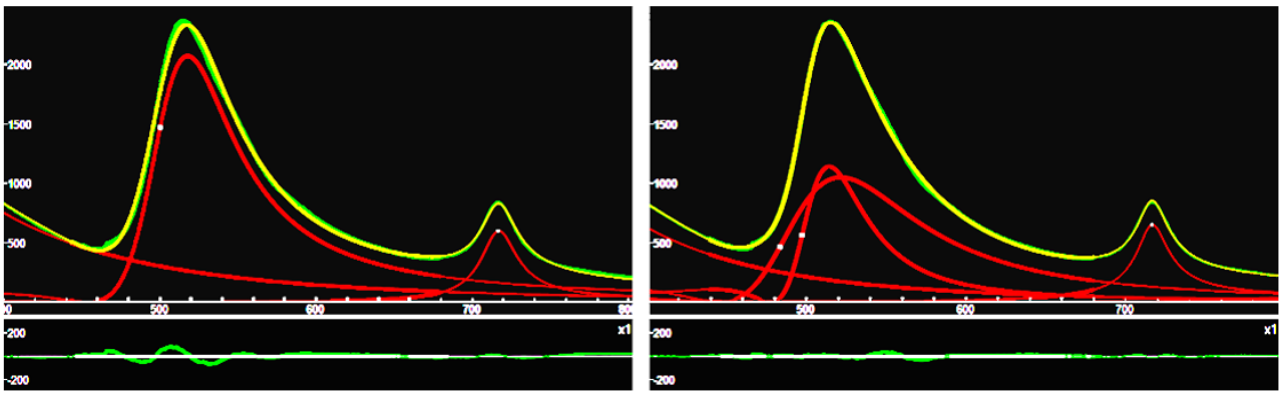

Fig.5: *Decompositions of the band at 515 cm^{-1}, assigned E(TO), A_1(TO) as in the Figure 1, with one or two q-BWF functions. On the left, the decomposition as in the Figure 2 previously given; on the right, a decomposition in two different components. Note that the misfit (lower part of images) is strongly reduced. The two components have the peaks at 514 and 526 cm^{-1}, respectively. The fit of the dip, that in the Figure 1 is assigned to E(LO), A_1(LO), E(TO) is improved too.*

We have previously told that, with the q-BWF functions, we have the possibility of decomposing the spectrum in a few components. The q-BWF function work well because of their asymmetric shape, coupled with the broadening role played by the q parameter in the q-exponential. However, we could ask ourselves if the use of symmetric components is suitable or not for decomposing $BaTiO_3$ spectra. That is, for the specific band in the Figure 5, can we use symmetric functions for decomposing it? Let us try with the q-Gaussian functions, that is the q-BWF functions with xi=0. In the Figure 6, the comparison is given. On the right of Fig.6 we can see

that two q-Gaussians cannot properly describe the asymmetry of the band. Even adding two further q-Gaussian components we do not improve the fit, that is, the misfit remains significant.

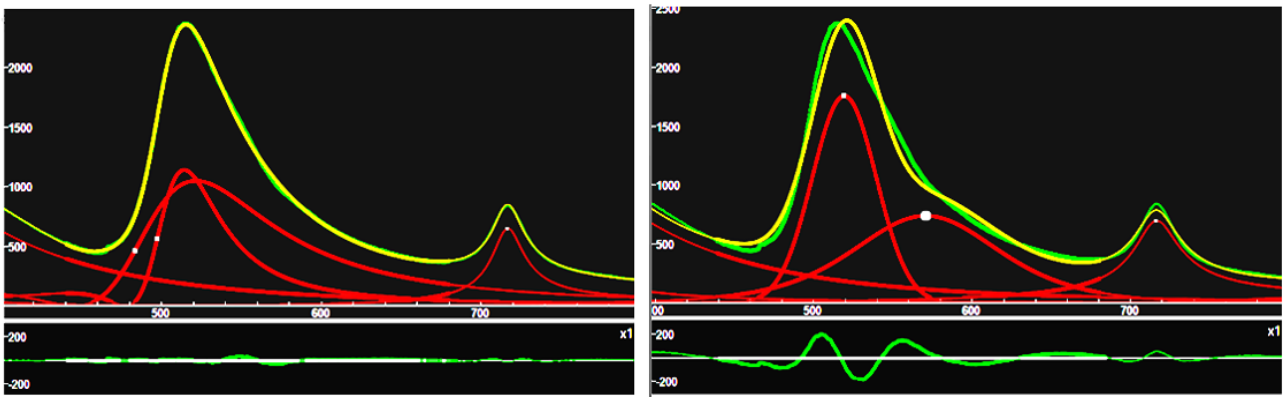

Fig.6*: Decompositions of the band at 515 cm^{-1}, as in the Figure 1. On the left, the decomposition as in the Figure 5 previously given on the right, in two different components. On the right, the decomposition obtained with two q-Gaussian symmetric functions. Note that the misfit is quite large. The two q-Gaussian components have the peaks at 519 and 570 cm^{-1}, respectively.*

To conclude this discussion, let us remember that Ferrari and Robertson, 2000, contemplated the BWF function as suitable to describe asymmetries in the case of the Raman spectroscopy of carbonaceous material. Let us stress that here we generalized this function, using the q-exponential instead of the exponential, as we proposed in 2023. The q-parameter can tune the shape from Lorentzian to Gaussian. In fact, we can have also over-Lorentzian behaviors, when q-parameter is greater than 2.

About Fano resonance, or Fano interference, we must further consider literature. Let us stress that the "Fano line shape" is the BWF (Breit Wigner Fano) function.

Interference effect

Pinczuk et al. proposed the "Raman scattering by polaritons in tetragonal $BaTiO_3$". According to the researchers, their data "also exhibit the interference effect on the 170 cm^{-1} mode previously identified by Rousseau and Porto. This was assigned to an interference between first and second order bands. In view of [their] results concerning the mode at 270 cm^{-1}, the possibility has to be considered that the interference occurs between (bands corresponding to) two $q \approx 0$ TO phonons. Such an interference can occur when the two TO phonons are anharmonically coupled to the same (two or more) acoustical phonons" (Pinczuk et al., 1969).

In Rousseau and Porto, 1968, we find that "when a discrete energy state is superimposed on a broad continuum, the well-known phenomenon of resonant interference (Auger processes) may occur. In general, Auger interactions are characterized by … broadening and distortion of the absorption, emission, and scattering line shapes". And "the quantum mechanical formalism describing Auger transitions has been thoroughly developed by Fano and Cooper" (Rousseau & Porto, 1968). In their Letter, Rousseau and Porto illustrate "the Raman-scattering observation of a resonant interference between one- and two-phonon states of $BaTiO_3$" and show that "this interference may be completely described by the Fano formalism for Auger processes".

"The particular importance offered by Raman spectroscopic observation of such processes is the ability to select a diversity of phonon propagation directions and differential polarizability tensors, and thereby drastically vary the degree of interference" (Rousseau & Porto, 1968).

Temperature evolution of Fano line shape

Zheng and coworkers, 2023, propose the "temperature evolution of the Fano line shape in the Raman spectra of $BaTiO_3$ nanoparticles". In the introduction, the researchers tell that "Fano line shape is one of the distinct characteristics for the quantification of solid materials. However, as the pervasive application of barium titanate, the industry application of Fano resonance mechanism has not been that popular" (Zheng et al. mentioning Dwij et al. 2021). "According to the Raman spectra of $BaTiO_3$, many researchers have observed the interesting phenomenon of Fano resonance around 185 cm^{-1}, which is due to the interference of a discrete energy level and a continuous band/states. For example, Rousseau et al. and Porto et al. reported the asymmetric Raman peak around 175 cm^{-1} under different polarization configurations at room temperature (RT) in $BaTiO_3$ crystal. They attributed this asymmetric Fano line shape to the energy overlap between a discrete one-phonon process and a broad two-acoustic-phonon scattering, leading to a negative asymmetric factor q [here, our xi]). Other mechanisms of the Fano resonance have been proposed in previous studies, for example, by Pinczuk et al. as the anharmonic coupling of two TO phonons via acoustical phonons in BaTiO3 crystal at RT; by Pradhan et al. as the coupling between a discrete $A_1(LO_1)$ phonon and a central peak due to rapid polarization fluctuations in polar nano regions in Co-doped BaTiO3 crystal at RT. The detailed mechanism of the Fano resonance is still under debate and is worth further investigation" (Zheng et al., 2023). In the Table I by Zheng and coworkers we find the "possible explanations of Fano peak origin", according to Dwij et al., Pradhan et al. , Venkateswaran et al., Pinczuk et al. and Rousseau and Porto.

Zheng and coworkers "conducted a detailed temperature-dependent Raman scattering study of $BaTiO_3$ nanoparticles from 4 to 297 K, to analyze the temperature evolution of the asymmetric peak around 185 cm^{-1}. By fitting with the Fano line shape function, [Zheng and coworkers] attempted to link the parameters in the Fano line shape function to the phase change of $BaTiO_3$. [The researchers] found that the temperature evolution of the Fano peak helps confirm the coupling of the central peak and an A(TO) mode, which is the possible origin of Fano resonance in $BaTiO_3$ nanoparticles studied [by Zheng and coworkers]". The Fano dip considered is at 185 cm^{-1}. The $BaTiO_3$ nanoparticle powders studied by Zheng and coworkers had been synthesized and provided by Huizhou Bao Shun Mei Technology Co. Ltd. The Raman instrument was a confocal micro-Raman Horiba, LabRAM HR evolution, with a 532 nm excitation laser. The spectral resolution of the Raman system is better than 1 cm^{-1} (Zheng et al., 2023).

In the Figure 3 by Zheng et al. we can see a Fano line, with a peak which seems centered at 185 cm^{-1}, and a range from 178 to 196 cm^{-1}, and a shift of intensity values. Let us conclude trying to investigate the spectra from RRUFF and ROD database to evidence the same Fano resonance. The only spectrum we can use is that from ROD, 3500224, laser 633 nm, in the range from 160 to 200 cm^{-1}. In the following Fig.7, the fit of the data are proposed with a q-BWF function (on the left) and q BWF of the right. The q-BWF function as an over-Lorentzian asymmetric behavior.

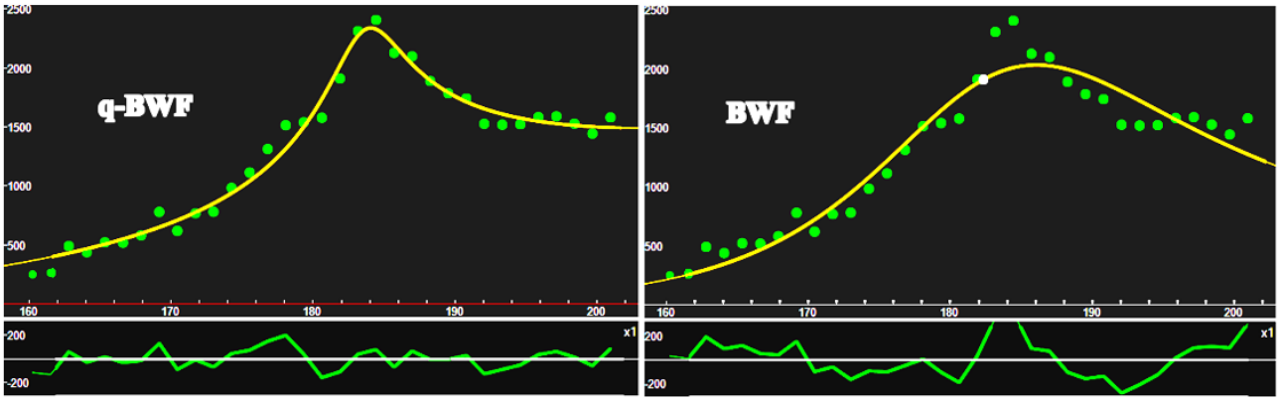

Fig.7. *Fit of data ROD 3500224, laser 633 nm, range from 160 to 200 cm^{-1}. On the left, a q-BWF function is used, on the right, the classic BWF function.*

The result proposed in the Figure 7, on the left, is quite good. However, we have no information about the size of particles. Moreover, ROD tells that the space group of the sample is P2mm, that is orthorhombic. Therefore, a further study that we can make is that of decomposing the Raman spectra of tetragonal, orthorhombic and rhombohedral $BaTiO_3$, such as those shown by Tyagi et al., 2018. The Figure 3 of their article gives relevant differences, and therefore we expect different behaviors of q-BWF functions.

References

1. Aksel, E., & Jones, J. L. (2010). Advances in lead-free piezoelectric materials for sensors and actuators. Sensors, 10(3), 1935-1954.
2. Bahri, F., & Khemakhem, H. (2014). Raman and dielectric investigation of (Ba0. 9− xSrxCa0. 1)(Ti0. 8Zr0. 2) O3 ferroelectric ceramics. Ceramics International, 40(6), 7909-7913.
3. Burns, G., & Scott, B. A. (1971). Raman scattering in the ferroelectric system Pb1− xBaxTiO3. Solid State Communications, 9(11), 813-817.
4. Dwij, V., De, B. K., & Sathe, V. G. (2021, May). Electric field tuning of the Fano resonance in BaTiO3. In 2021 IEEE International Symposium on Applications of Ferroelectrics (ISAF) (pp. 1-4). IEEE.
5. El Mendili, Y., Vaitkus, A., Merkys, A., Gražulis, S., Chateigner, D., Mathevet, F., Gascoin, S., Petit, S., Bardeau, J.F., Zanatta, M., & Secchi, M. (2019). Raman Open Database: first interconnected Raman–X-ray diffraction open-access resource for material identification. Journal of applied crystallography, 52(3), pp.618-625.
6. Fano, U., & Cooper, J. W. (1965). Line profiles in the far-uv absorption spectra of the rare gases. Physical Review, 137(5A), A1364.
7. Ferrari, A. C., & Robertson, J. (2000). Interpretation of Raman spectra of disordered and amorphous carbon. Physical Review B 61: 14095–14107.
8. Hayashi, H., Nakamura, T., & Ebina, T. (2013). In-situ Raman spectroscopy of BaTiO3 particles for tetragonal–cubic transformation. Journal of Physics and Chemistry of Solids, 74(7), 957-962.
9. Huang, T. C., Wang, M. T., Sheu, H. S., & Hsieh, W. F. (2007). Size-dependent lattice dynamics of barium titanate nanoparticles. Journal of Physics: Condensed Matter, 19(47), 476212.
10. Jiang, Y. J., Zeng, L. Z., Wang, R. P., Zhu, Y., & Liu, Y. L. (1996). Fundamental and Second-Order Raman Spectra of BaTiO3. Journal of Raman spectroscopy, 27(1), 31-34.
11. Kumar, A., Cassetta, M., El Mendili, Y., Zanatta, M., Daldosso, N., & Mariotto, G. (2018). Raman spectrum of commercial BaTiO3. Personal communication to ROD, 2018
12. Lafuente, B., Downs, R. T., Yang, H., & Stone, N. (2015). 1. The power of databases: The RRUFF project. In Highlights in mineralogical crystallography (pp. 1-30). De Gruyter (O).
13. Lee, H. W., Moon, S., Choi, C. H., & Kim, D. K. (2012). Synthesis and size control of tetragonal barium titanate nanopowders by facile solvothermal method. Journal of the American Ceramic Society, 95(8), 2429-2434.
14. Ma, C., & Rossman, G. R. (2008). Barioperovskite, BaTiO3, a new mineral from the Benitoite Mine, California. American Mineralogist, 93(1), 154-157.
15. Maxim, F., Vilarinho, P. M., Ferreira, P., Reaney, I. M., & Levin, I. (2011). Kinetic study of the static hydrothermal synthesis of BaTiO3 using titanate nanotubes precursors. Crystal growth & design, 11(8), 3358-3365.
16. Noma, T., Wada, S., Yano, M., & Suzuki, T. (1996). Analysis of lattice vibration in fine particles of barium titanate single crystal including the lattice hydroxyl group. Journal of applied physics, 80(9), 5223-5233.
17. Parmar, V. B., Raval, D., Gupta, S. K., Gajjar, P. N., & Vora, A. M. (2023). BaTiO3 perovskite for optoelectronics application: A DFT study. Materials Today: Proceedings.
18. Pasha, U. M., Zheng, H., Thakur, O. P., Feteira, A., Whittle, K. R., Sinclair, D. C., & Reaney, I. M. (2007). In situ Raman spectroscopy of A-site doped barium titanate. Applied physics letters, 91(6).

19. Pinczuk, A., Burstein, E., & Ushioda, S. (1969). Raman scattering by polaritons in tetragonal BaTiO3. Solid State Communications, 7(1), 139-142.
20. Pradhan, D.K., Mohanty, H.S., Kumari, S., Bhoi, K., Tang, N., Rahaman, M.M., Pradhan, D.K., Kumar, A., Gilbert, D.A., & Rack, P.D. (2021). Ferroic phase transitions and magnetoelectric coupling in cobalt doped BaTiO 3. Journal of Materials Chemistry C, 9(37), pp.12694-12711.
21. Rimai, L., Parsons, J. L., Hickmott, J. T., & Nakamura, T. (1968). Raman spectrum of long-wavelength phonons in tetragonal barium titanate. Physical Review, 168(2), 623.
22. Rousseau, D. L., & Porto, S. P. S. (1968). Auger-Like Resonant Interference in Raman Scattering from One-and Two-Phonon States of BaTi O 3. Physical Review Letters, 20(24), 1354.
23. Shiratori, Y., Pithan, C., Dornseiffer, J., & Waser, R. (2007). Raman scattering studies on nanocrystalline BaTiO3 Part I—isolated particles and aggregates. Journal of Raman Spectroscopy: An International Journal for Original Work in all Aspects of Raman Spectroscopy, Including Higher Order Processes, and also Brillouin and Rayleigh Scattering, 38(10), 1288-1299.
24. Scalabrin, A., Chaves, A. S., Shim, D. S., & Porto, S. P. S. (1977). Temperature dependence of the A1 and E optical phonons in BaTiO3. physica status solidi (b), 79(2), 731-742.
25. Sendova, M., Hosterman, B. D., Raud, R., Hartmann, T., & Koury, D. (2015). Temperature-dependent, micro-Raman spectroscopic study of barium titanate nanoparticles. Journal of Raman Spectroscopy, 46(1), 25-31.
26. Sherlin Vinita, V., Gowri Shankar Rao, R., Samuel, J., Shabna, S., Joslin Ananth, N., Shajin Shinu, P.M., Suresh, S., Samson, Y., & Biju, C.S. (2022). Structural, Raman and optical investigations of barium titanate nanoparticles. Phosphorus, Sulfur, and Silicon and the Related Elements, 197(3), pp.169-175.
27. Sparavigna, A. C. (2023). Asymmetric q-Gaussian functions generalizing the Breit-Wigner-Fano functions. Zenodo. https://doi.org/10.5281/zenodo.8356165
28. Sparavigna, A. C. (2024). Molybdenum Disulfide MoS2 and the q-BWF line shapes (Raman Spectroscopy). ChemRxiv. doi:10.26434/chemrxiv-2024-cprs3-v3
29. Sparavigna, A. C. (2024). Raman Broad Scans of Rare Earth Oxide (REO) Glasses from RRUFF Database, Compared to the Raman spectra of RE Oxides from Raman Open Database. International Journal of Sciences, 13(07), 52-64. http://dx.doi.org/10.18483/ijSci.2780
30. Sun, Q., Gu, Q., Zhu, K., Jin, R., Liu, J., Wang, J., & Qiu, J. (2017). Crystalline structure, defect chemistry and room temperature colossal permittivity of Nd-doped barium titanate. Scientific reports, 7(1), 1-8.
31. Tyagi, S., Sathe, V. G., Sharma, G., Srihari, V., & Poswal, H. K. (2018). Evidence of low-symmetry phases in pressure-dependent Raman spectroscopic study of BaTiO 3. Journal of materials science, 53, 7224-7232.
32. Tsallis, C. (1988). Possible generalization of Boltzmann-Gibbs statistics. Journal of statistical physics, 52, 479-487.
33. Wada, S., Suzuki, S., Noma, T., Suzuki, T., Osada, M., Kakihana, M., Park, S.E., Cross, L.E., & Shrout, T.R. (1999). Enhanced piezoelectric property of barium titanate single crystals with engineered domain configurations. Japanese journal of applied physics, 38(9S), p.5505.
34. Wojdyr, M. (2010). Fityk: a general-purpose peak fitting program. Journal of applied crystallography, 43(5), 1126-1128.
35. Zhang, W. H., Chen, L., Tao, Y. T., Chen, J., & Zhang, J. X. (2011). Raman study of barium titanate with oxygen vacancies. Physica B: Condensed Matter, 406(24), 4630-4633.
36. Zheng, Y., Zhao, Y., Yu, J., Lu, W., Ning, J., & Zheng, C. (2023). Temperature evolution of the Fano line shape in the Raman spectra of BaTiO3 nanoparticles. Applied Physics Express, 16(3), 032003.